Vibrational signatures of isotopic impurities and complexes in II-VI compound semiconductors

Devki N. Talwar*
Department of Physics, Indiana University of Pennsylvania, 975 Oakland Avenue, 56 Weyandt Hall, Indiana, Pennsylvania 15705-1087, USA

Zhe Chuan Feng
Institute of Photonics and Optoelectronics, Department of Electrical Engineering, and Center for Emerging Material and Advanced Devices, National Taiwan University, Taipei 106-17, Taiwan, ROC

Tzuen-Rong Yang
Department of Physics, National Taiwan Normal University, Taipei 106-11, Taiwan, ROC
(Received 28 November 2011; revised manuscript received 19 April 2012; published 8 May 2012)

In II-VI compound semiconductors, we have used a comprehensive Green's function theory to study the vibrational properties of isotopic defects and to ascertain the microstructure of complex centers involving dopants and intrinsic impurities. The phonons generated by a realistic lattice-dynamical model for the host materials are integrated in simulating the Green's functions to help explicate the observed localized vibrational modes (LVMs) for various defect centers. Contrary to the distinct force constants required for isolated defects, the isotopic shift of LVMs has offered strong revelations for inflexible 'impurity-host' interactions in each isotopic defect. In compound semiconductors a unique force variation correlation with bond covalency is proposed providing corrections to the nearest-neighbor (NN) force constants for the closest mass isoelectronic and impurities carrying static charges. The articulation is extremely useful for defining perturbations and for analyzing the infrared absorption data on LVMs of complex defect centers. In corroboration with experiments, the Green's functions theory of impurity modes in Li-doped CdTe:Al (ZnSe:Al) has established second NN $Li_{Cd(Zn)}$-$Al_{Cd(Zn)}$ pairs indicating the passivation of group-I acceptors via interaction with group-III elements as donors. The proposal of an antisite complex model Al_{Zn}-Zn_{Se}-Al_{Zn} for the X center is consistent with the existing absorption results on impurity modes and is equally justified by theoretical considerations—making it the more likely identity for the native defect compensating neighboring Al_{Zn} donors in ZnSe.

DOI: 10.1103/PhysRevB.85.195203 PACS number(s): 78.20.−e, 63.20.Pw, 63.22.−m, 78.67.−n

I. INTRODUCTION

The II-VI compounds of zinc and cadmium (Zn-Cd) chalcogenides with direct band gaps (1.47–3.91 eV) constitute a technologically important family of materials for microelectronic, photonic, and integrated optoelectronic applications.[1–8] The ability to prepare mixed alloys with arbitrary composition of group IIB cations (e.g., Zn, Cd, and Hg) replacing group IIB ions as in $Hg_{1-x}Zn_xA$ (A = Se, Te, S), or group IIA (e.g., Be, Mg, Ca, Ba) cations as in $Zn_{1-x}Mg_xA$, has opened up many possibilities of investigating their structural,[9–16] electronic,[13,14] and lattice dynamical properties.[17–24] The II-VI binary compounds and/or ternary alloys will not be of much practical use if they cannot be doped. However, the fabrication of p-n junctions, indispensable for commercial optoelectronic devices, has been hampered by the doping impediments. Despite several decades of extensive research, it is still not very clear as to why some of the wide-band-gap II-VI compound semiconductors (including ZnSe) can be made n type but not p type while others (ZnTe) can be doped p type but not n type. The mechanism of this predicament still remains a mystery. For p-type doping in II-VI materials one expects group I (Li, Ag, Au) or group V (N, P) elements to form shallow acceptors (a^-) and for n-type doping group III (Al, Ga, In) elements to create shallow donor (d^+) levels. However, Zn-Cd chalcogenide materials heavily doped with Li_{II} (a^-), N_V (a^-), P_V (a^-), and Al_{II} (d^+) are highly compensated by native defects—the nature of compensating centers still remains largely unknown. As the masses of Li, N, P, and Al are much lighter than those of the group II and group VI elements of the host crystals, the infrared absorption and/or Raman scattering studies of localized vibrational modes (LVMs) integrated with the realistic lattice dynamical Green's function calculations can provide an attractive opportunity of (a) identifying the site selectivity of both isolated and complex defect centers with expected symmetries and (b) monitoring the shifts of defect modes by changing the isotopic composition of impurity species.

It is to be noted that in binary II-VI compounds with a gap between their acoustic and optical phonon bands (e.g., ZnS, ZnSe, ZnTe, CdTe, and CdSe), a substitutional impurity may give rise to either one or two nonpropagating infrared active vibrational modes.[25] For instance, if the impurities of light mass replace the lighter host lattice atoms in a compound semiconductor they may produce the LVMs at frequencies ω_{LVMs} higher than the maximum phonon (ω_m) frequency of the perfect lattice. On the other hand, it is also possible that a light impurity occupying the heavier host atom can give rise to both a high frequency ω_{LVM} and a gap-mode (ω_g), which may fall between the gap of the host lattice phonon bands. In compound semiconductors the gap modes are also expected when heavier impurities occupy the light host atoms' sites.[25] While a gap mode $\omega_g \sim 159.2$ cm^{-1} (232 cm^{-1}) in ZnSe (ZnS) is detected for a heavier isoelectronic barium (selenium) impurity occupying the lighter zinc (sulphur) host atom, i.e., Ba_{Zn} (Se_S), the local ω_{LVM} and gap ω_g modes of light sulphur impurities substituting for the heavier tellurium sites

S_{Te} in Cd*Te* (247.5 and 106.1 cm^{-1}) and Zn*Te* (∼415 and 144.6 cm^{-1}) have been suggested.[19,20] Moreover, the isotopic shifts of the ω_{LVMs} caused by the light isoelectronic impurities Mg^{2+}; Ca^{2+} occupying the cation sites; and O^{2-}, S^{2-}, and Se^{2-} substituting for the anion sites in II-VI compounds have also been observed.[19,20]

For nonisoelectronic defects, several experimental measurements of the LVMs exist in the literature for both isolated Al (d^+) donors,[21,22] Li (a^-),[21–24] P (a^-),[22–24] N (a^-)[18] acceptors, and complex centers comprising Al (Ga or In) + Li or Al (Ga or In) + P impurities in Zn-Cd chalcogenides.[21–24] Unfortunately, the analyses of such studies still remain either incomplete or inconsistent. Although the isolated Al_{II} (P_{VI}, N_{VI}) defects in II-VI compound semiconductors form substitutional effective mass-type donors (acceptors), the possibility that these impurities may also create complex centers involving intrinsic defects in heavily doped samples have been suggested.[21–24] For instance, in the as-grown state, Al-doped II-VI materials are in general highly compensated—revealing lower carrier density than the actual concentration of Al dopants. This means that the charge of Al donor (Al_{II}) is neutralized by self-generated intrinsic (e.g., vacancy and/or antisite) defects carrying charges of opposite sign. Consequently in ZnSe:Al the creation of *X* centers involving Al (d^+) donors and intrinsic defects complicates the analyses of infrared absorption spectra of impurity vibrational modes.[21,22] An earlier success of exploiting Li as a compensating species in doped III-V compound semiconductors prompted its use in Al-doped II-VI materials to help elucidate the LVM data.[21–24] Double doping with column V elements (e.g., P, As, Sb) has also assisted in ascertaining the vibrational modes of the donor-acceptor pairs in Al-doped II-VI compounds.[22–24] In Zn-Cd chalcogenides, although the majority of the results on LVMs for both isolated charged (d^+ or a^-) impurities and complex defect centers involving donors and acceptors are obtained from the absorption bands by using the Fourier transform infrared (FTIR)[17,18,20–24] spectroscopy, the impurity modes have also been detected as phonon sidebands in the photoluminescence (PL) absorption and as Raman-active modes in the Raman scattering spectroscopy.[25]

From a theoretical stand point, Biernacki *et al.*[26] used a phenomenological two-particle potential within the tight-binding approximation and calculated the isotopic shifts of LVMs for isoelectronic Mg^{2+} and S^{2-} defects in ZnTe and CdTe. Unfortunately, this approach cannot be used for predicting the gap modes of S_{Te} in ZnTe and CdTe and/or Ba_{Zn} in ZnTe. Another theoretical attempt made recently by Zhang *et al.*[27] is to apply the density functional theory (DFT) to interpret the FTIR data of impurity modes associated with O impurities in CdTe.[17] Although the calculated result of ω_{LVM} for an isolated O_{Te} is in good agreement with the experimental data, the simulated frequencies of LVMs for the nearest-neighbor (NN) O_{Te}-V_{Cd} pair-defect in CdTe are found, however, much lower than the observed values from infrared spectroscopy.[17] For establishing the role of charged defects in II-VI compounds despite the availability of extensive atypical FTIR data[21–24] on LVMs, the microscopic structure of complex centers involving Al-donors and native defects (especially *X* centers in ZnSe:Al) as well as donor-acceptor pairs has not been fully ascertained either by phenomenological[26] or DFT methodologies.[27]

The purpose of the present work is to use a realistic lattice dynamical method and undertake a comprehensive theoretical study to address some of the important issues related to the vibrational characteristics of both isoelectronic and charged impurity complexes in II-VI compound semiconductors. In this approach we have adopted a rigid-ion model (RIM)[28] to describe the interatomic interactions of the host crystals while the impurity modes caused by defects are simulated within the Green's functions formalism.[29,30] It is to be noted that the knowledge of accurate eigenvalues and eigenvectors displaying the correct phonon dispersions as well as precise phonon gaps between the acoustic and optic phonon bands is crucial *per se* for understanding the interatomic forces of the host lattices, assessing impurity-host interactions and predicting impurity modes.[31] We must accentuate that for studying the dynamical properties of defects, the Green's function theory has clearly offered the delineation of chemical trends by attaining a simple physical understanding of the bonding situation through general magnitude of the impurity-host interactions. Here, we reaffirm that the method can be used successfully to elucidate not only the observed isotopic shifts of impurity modes for various isolated defects[18–20] but also it can help ascertain the microstructure of complex defect centers involving Al (Ga or In) + Li or Al (Ga or In) + P and/or intrinsic defects responsible for the atypical LVM data in II-VI compound semiconductors.[21–24] For the O impurities in CdTe our simulations of the local modes have provided strong corroborations to the recent DFT calculations[27] challenging the proposed assignment of the two high frequency modes (ω_1, ω_2) to the NN O_{Te}-V_{Cd} pair-defect of C_{3v}-symmetry.[17]

This paper is organized as follows. Starting with a brief outline of the general theory in Sec. II, we have reported the procedure exploiting RIM to study the lattice dynamics of zinc-blend-type (cf. Sec. II A) II-VI materials. A succinct description is presented in Secs. II B and II C for the perfect and imperfect lattice Green's functions—leading to the Dyson equation required for examining the impurity induced vibrational modes. Assuming that the atomic interactions in compound semiconductors are not strongly affected by the presence of defects, the effects may be described as a small perturbation arising from the changes in atomic masses and NN force constants. In the framework of a RIM[28] we have described the perturbation matrices (cf. Sec. II D) of various defect centers in zinc-blend-type materials by including both the mass change at the impurity sites as well as the variations in the NN force constants between impurity-host atoms. In the subsections of II D1–3, we emphasized the use of group-theoretical arguments to block-diagonalize the perturbation and host lattice Green's functions matrices associated with (a) a single isolated defect of T_d symmetry, (b) an NN pair-defect of C_{3v} symmetry, and (c) a complex-defect center of C_s or C_{2v} symmetry. In defining the perturbation matrices we have not considered the variations in the Coulomb interactions, as their long range will render the Green's function approach intractable. Theoretical results of lattice dynamics for the perfect II-VI materials are summarized in Sec. III A. Numerical calculations of LVMs are reported in Sec. III B with emphasis on single substitutional isotopic defects (see Sec. III B1) occupying either anion or cation sites. The trends of force variations for the isolated charged impurities are analyzed in Sec. III B2.

The results are reported for the dynamical properties of NN pair-defects in Sec. III C—highlighting the LVMs of donor-acceptor pairs in II-VI compounds (Sec. III C1). In Sec. III C2 the simulated results of impurity modes for second NN complex centers of C_s and C_{2v} symmetries are compared with the existing experimental data. By Green's function theory and considering various pertinent models, we have designated a microstructure of a second NN complex center (X center), which best explains the observed atypical LVMs and is a more likely identity for the native defect-compensating neighboring Al_{Zn}-donors in ZnSe.[21,22] Theoretical results are compared and discussed in the context of existing experimental data[21–24] from the infrared absorption spectroscopy with summary and concluding remarks presented in Sec. IV.

II. TECHNICAL MATTERS

To extract the nature of impurity-host bonding from the existing spectroscopy data on LVM in semiconductors, two equally reliable theoretical efforts have been made in recent years:[27,31] (a) A *microscopic* analysis is used based on DFT within the local density approximation[27] to estimate the phonon energies of both perfect and imperfect systems, and (b) a *macroscopic* analysis is considered based on the general treatment of lattice dynamics in terms of interatomic forces by using Green's function theory[31]—the displacement response to the sinusoidal driving forces in perfect/imperfect lattice has been estimated. The former approach generally requires a heavy computation for isoelectronic defects, and presumably it is much more cumbersome for nonisoelectronic (charged) defects. Except for the recent *first-principles* calculations of impurity modes in CdTe:O,[27] the nature of impurity-host bonding by *ab initio* methods has yet to be extracted for the Al (d^+) donors and Li (a^-), P (a^-) acceptors in CdTe or ZnSe.[21–24] On the other hand, Green's function theory (cf. Secs. II B and II C) can be applied for empathizing the dynamical properties of both isoelectronic and charged defects in compound semiconductors.[31] The advantage of the second approach over the first one is that it allows the coupling of the vibrations of the defect centers to the bulk materials. By taking into account the symmetry of the system and using group-theoretical arguments one can clearly visualize which types of impurity modes are optically active and remain localized around the defects.[32,33] A comprehensive account of the dynamical properties for imperfect lattices by Green's function technique has been discussed in several review articles,[24,25] monographs,[31] and books.[29] Our discussion here to treat the impurity vibrations in II-VI compound semiconductors is therefore very brief and only for the purpose of establishing the notations to be used throughout the paper.

A. Rigid-ion model (RIM)

In the harmonic approximation the invariance of potential energy with respect to the rigid-body translations, rotations, and symmetry operations require a minimum of two NN force constants (A, B) to treat the lattice dynamics of zinc-blend-type materials. The calculations of GaAs by Grimm *et al.*[34] based on this two-parameter force model, however, failed to understand the experimental phonon dispersions.[35] This suggested the need to improve the two-parameter force model by including interactions with more distant neighbors. Clearly the RIM proposed by Kunc[28] is a step in that direction. The model takes into account both the short-range interactions (up to and including second NN) and long-range Coulomb effects arising from the electrostatic forces. The quantities of interest in the RIM are the force constant $\overleftrightarrow{\phi}^{sC}(\equiv\overleftrightarrow{\phi}^{s}+\overleftrightarrow{\phi}^{C})$ and dynamical $\overleftrightarrow{D}^{sC}(\equiv\overleftrightarrow{D}^{s}+\overleftrightarrow{D}^{C})$ matrices. From the tetrahedral (T_d) symmetry of zinc-blend lattices, the off-diagonal Cartesian blocks of the short-range $\overleftrightarrow{\phi}^{s}$ force constant matrix between NN is shown to have the form[28]

$$\langle l\kappa|\phi^{s}|l\kappa'\rangle = \begin{pmatrix} A & B & B \\ B & A & B \\ B & B & A \end{pmatrix}, \tag{1}$$

while the force constant matrices $\overleftrightarrow{\phi}^{s}$ between the second NNs are given by[28]

$$\langle l\kappa|\phi^{s}|l\kappa\rangle = \begin{pmatrix} C_\kappa & D_\kappa & \pm E_\kappa \\ D_\kappa & C_\kappa & \pm E_\kappa \\ \pm E_\kappa & \pm E_\kappa & C_\kappa \end{pmatrix}; \quad \text{with} \quad \kappa = 1,2. \tag{2}$$

Here, l labels the basic unit cells with κ representing the two atoms in each cell. For evaluating the elements of long-range Coulomb force constant $\overleftrightarrow{\phi}^{C}$ matrix, one requires an additional parameter Z (the effective charge).[28] In this generalized RIM the atomic displacements u of each jth mode are considered to have a sinusoidal spatial dependence thus allowing a unique wave vector $\vec{q}$ to be associated with each mode frequency $\omega_j(\vec{q})$:

$$u_\alpha(l\kappa|\vec{q}\,j) = (M_\kappa)^{-1/2} e_\alpha(\kappa|\vec{q}\,j)\exp i[\vec{q}\vec{x}(l\kappa) - \omega_j(\vec{q})t]; \quad \text{with} \quad \alpha = x,y,z. \tag{3}$$

Again, the components of eigenvectors $e_\alpha(\kappa|\vec{q}\,j)$ for each mode frequency $\omega_j(\vec{q})$ satisfy the familiar orthogonality

$$\sum_{\alpha\kappa} e^{*}_\alpha(\kappa|\vec{q}\,j)e_\alpha(\kappa|\vec{q}\,j') = \delta_{jj'} \tag{4}$$

and closure relations

$$\sum_{j} e^{*}_\alpha(\kappa'|\vec{q}\,j)e_\beta(\kappa|\vec{q}\,j) = \delta_{\alpha\beta}\delta_{\kappa\kappa'}. \tag{5}$$

In the framework of a RIM the lattice vibrations of zinc-blend materials in the harmonic approximation are obtained by solving the equation of motion

$$\omega^2_j(\vec{q})e_\alpha(\kappa|\vec{q}\,j) = \sum_{\kappa'\beta} D^{sC}_{\alpha\beta}(\kappa\kappa'|\vec{q})e_\beta(\kappa'|\vec{q}\,j), \tag{6}$$

where

$$D^{sC}_{\alpha\beta}(\kappa\kappa'|\vec{q}) = D^{s}_{\alpha\beta}(\kappa\kappa'|\vec{q}) - \frac{Z_\kappa Z_{\kappa'} e^2}{(M_\kappa M_{\kappa'})^{1/2}} D^{C}_{\alpha\beta}(\kappa\kappa'|\vec{q}). \tag{7}$$

The elements of dynamical matrices $\overleftrightarrow{D}^{s}$ and $\overleftrightarrow{D}^{C}$ describing the general short- and long-range Coulomb interactions have been reported elsewhere.[36] In II-VI compound semiconductors as the primitive unit cell contain two atoms, Eq. (6) creates an

eigenvalue problem of dimension (6×6). The values of wave vectors $\vec{q}$ restricted to lie within the first Brillouin zone of the fcc lattice assume the form

$$|\vec{q}| = \frac{\pi}{a_o}(q_1,q_2,q_3);\ -1 \leqslant q_1,q_2,q_3 \leqslant 1;\ q_1+q_2+q_3| \leqslant \frac{3}{2} \tag{8}$$

with triplets (q_1,q_2,q_3) distributed uniformly throughout the volume of the Brillouin zone.

Once the RIM is optimized[36] for the perfect materials the eigenvalue equation [Eq. (6)] is solved numerically for each $\vec{q}$-vector in the Brillouin zone to obtain the lattice phonons (eigenvalues and eigenvectors). The accuracy of RIM is tested by comparing the simulated phonon dispersions (i.e., the plots of $\omega_j(\vec{q})$ vs $\vec{q}$)[37] with the inelastic neutron scattering data for ZnS, ZnSe, ZnTe, and CdTe.[38,39] In addition to the lattice dynamics, many other physical quantities [e.g., C_v(T), Θ_D(T), etc.][40] obtained *a posteriori* for the perfect crystals achieving good agreement with the experimental data have given further support to the reliability of the RIM. It is to be noted that the host lattice phonons are required to obtain (a) the Green's function matrix $\overleftrightarrow{G}^o$ (cf. Sec. II B) elements of the perfect crystal and (b) the Green's function $\overleftrightarrow{G}$ (cf. Sec. II C) of the imperfect lattice in terms of $\overleftrightarrow{G}^o$ and $\overleftrightarrow{P}$ (Sec. II D) for studying the impurity modes.

B. The perfect lattice Green's functions

The general methodology for simulating the Green's functions to investigate the impurity vibrational modes in solids is reported in many standard books,[24,25] review articles,[29] and monographs.[30] In the framework of RIM we have defined the Green's function $\overleftrightarrow{G}^o$ of the perfect compound semiconductor in the matrix notation as[29,30]

$$(\overleftrightarrow{M}\,\omega^2 - \overleftrightarrow{\phi}^{sC})\,\overleftrightarrow{G}^o = \overleftrightarrow{I}\ , \tag{9}$$

where the eigenfrequencies of the host crystal are obtained by solving the equation

$$\det(\omega^2\ \overleftrightarrow{I}\ - \overleftrightarrow{D}^{sC}) = \det[\overleftrightarrow{G}^o(\omega)]^{-1}/\det[\overleftrightarrow{M}]. \tag{10}$$

The component form of the Green's function $\overleftrightarrow{G}^o$ matrix is defined as

$$\langle l\kappa|G^o_{\alpha\beta}(\omega)|l'\kappa'\rangle = \frac{1}{N(M_\kappa M_{\kappa'})^{1/2}} \sum_{\vec{q}\,j} \frac{e_\alpha(\kappa|\ \vec{q}\ j)e^*_\beta(\kappa'|\vec{q}\,j)}{(\omega+i0^+)^2-\omega^2_j(\vec{q})} \times \exp\{i\vec{q}[\vec{x}(l\kappa)-\vec{x}(l'\kappa')]\}, \tag{11}$$

where N denotes the number of wave vectors, and $\vec{x}(l\kappa)$ is the equilibrium position vector of the atom $(l\kappa)$. An infinitesimal positive imaginary addition to ω yields the retarded Green's function[29,30] when the sinusoidal time dependence is represented by $\exp(-i\omega t)$. Again, the elements of Green's functions are expressed in terms of its real and imaginary parts [cf. eq. (8.4.14) of Ref. 29—the real part $\langle l\kappa|\mathrm{Re}G^o_{\alpha\beta}(\omega)|l'\kappa'\rangle$ is the principal segment of Eq. (11), while the imaginary part $\langle l\kappa|\mathrm{Im}G^o_{\alpha\beta}(\omega)|l'\kappa'\rangle$ is given by

$$\langle l\kappa|\mathrm{Im}G^o_{\alpha\beta}(\omega)|l'\kappa'\rangle = \frac{\pi}{N(M_\kappa M_{\kappa'})^{1/2}} \sum_{\vec{q}\,j} e_\alpha(\kappa|\ \vec{q}\ j)e^*_\beta(\kappa'|\vec{q}\,j) \times \exp\{i\vec{q}[\vec{x}(l\kappa)-\vec{x}(l'\kappa')]\} \times \delta\big(\omega^2-\omega^2_j(\vec{q})\big). \tag{12}$$

Clearly, Eq. (12) becomes zero outside the bands of allowed phonon frequencies of the host crystal lattice. In the numerical calculations of the Green's functions we have followed the standard procedures—first obtaining the imaginary part from a sample of wave vectors $\vec{q}$ in the reduced Brillouin zone and then determining the real part via the links provided by the Kramers-Kronig relations.[29,30]

C. The imperfect lattice Green's functions

Similar to Sec. II B, one can write the Green's function matrix of the imperfect lattice $\overleftrightarrow{G}$ as[29,30]

$$[(\overleftrightarrow{M}+\Delta\ \overrightarrow{M})\omega^2 - (\overleftrightarrow{\phi}^{sC}+\Delta\ \overleftrightarrow{\phi}^{sC})]\ \overleftrightarrow{G}=\overleftrightarrow{I}\ , \tag{13}$$

or equivalently in the form of a Dyson equation,

$$\overleftrightarrow{G}\ (\omega) = [\overleftrightarrow{I}\ - \overleftrightarrow{G}^o(\omega)\ \overleftrightarrow{P}\ (\omega)]^{-1}\ \overleftrightarrow{G}^o(\omega), \tag{14}$$

where $\overleftrightarrow{P}\ (\omega)[\equiv -\Delta\ \overleftrightarrow{M}\ \omega^2 + \Delta\ \overleftrightarrow{\phi}^{sC}]$ is the perturbation matrix related to the defects. The terms $\Delta\ \overleftrightarrow{M}$ and $\Delta\ \overleftrightarrow{\phi}^{sC}[\equiv \Delta\ \overleftrightarrow{\phi}^{s} + \Delta\ \overleftrightarrow{\phi}^{C}]$ represent the mass- and force-constant change matrices, respectively. As the variation in the Coulomb interactions is set to zero (i.e., $\Delta\ \overleftrightarrow{\phi}^{C} = 0$), only the mass change at the impurity sites and the changes in the NN impurity-host interactions are included in defining the perturbation matrices (cf. Sec. II D) of various defect centers. The impurity modes are then obtained by solving the equation[29,30]

$$\det|\ \overleftrightarrow{I}\ - \overleftrightarrow{G}^o(\omega)\ \overleftrightarrow{P}\ (\omega)| = 0, \tag{15}$$

representing the poles of $\overleftrightarrow{G}\ (\omega)$ at energies either above the maximum phonon frequency or in the gap between the acoustic and optic bands of the host lattices. In simulating the defect modes of various impurity centers we took advantage (cf. Sec. IIID) of the symmetry-adapted algorithms, which helped compare the theoretical results with the spectroscopic data.[17–24]

D. Perturbation matrices

In any defect calculations the most important issue is to give an adequate representation to the impurity perturbation. For studying the dynamical behavior of defects with Green's function theory[31] we have constructed the perturbation matrices $[\overleftrightarrow{P}\ (\omega)]$ by appropriately considering the effects of lattice relaxation to account for the impurity-host interactions. In II-VI compound semiconductors, the lattice relaxation in the vicinity of substitutional impurities are estimated by using Harrison's semiempirical bond-orbital model.[41] In terms of the Hartee-Fock atomic term values, this method provides simple analytical expressions for the change in impurity-host and host-host bond energies and suggests a

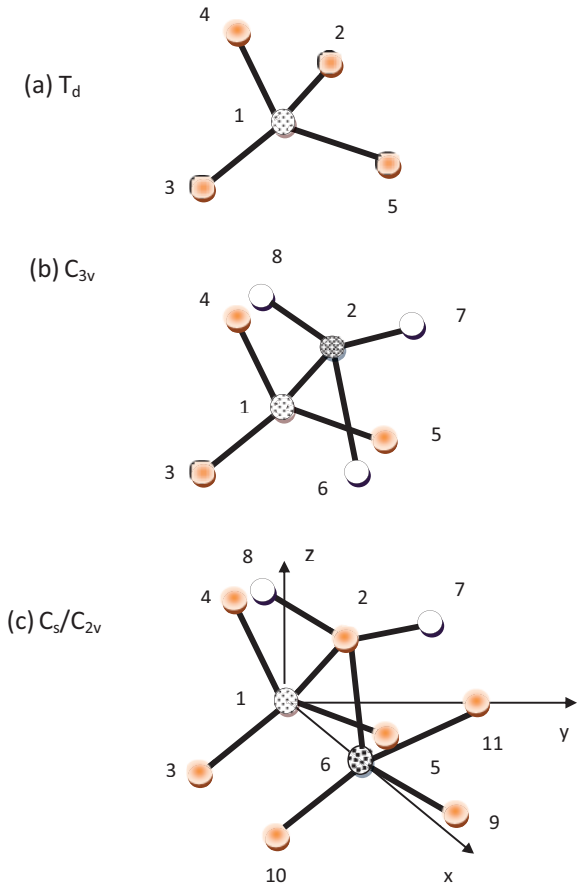

FIG. 1. (Color online) Perturbation models for (a) an isolated (T_d symmetry); (b) NN pair (C_{3v} symmetry); and (c) second NN complex centers (C_s/C_{2v} symmetry) in the zinc-blend-type compound semiconductors.

computationally efficient and reasonable way to estimate the bond-length distortions.[42] The perturbation matrices $\overleftrightarrow{P}(\omega)$ in the framework of RIM are then constructed following the method described in Ref. 43, i.e., by using the scaling properties of lattice relaxation with the variation of NN force constants along with the trends found in the short-range force constant matrix elements of the host crystals.[37]

1. Isolated defects: T_d symmetry

In II-VI compound semiconductors the simplest defect responsible for the LVMs is an isolated light substitutional impurity of point-group symmetry T_d [see Fig. 1(a)]—replacing either an atom of site II ($\kappa = 1$) or an atom of site VI ($\kappa = 2$). The perturbation $\overleftrightarrow{P}(\omega)$ matrix in the framework of a RIM includes both the changes in atomic masses at the defect sites as well as the NN force constants (cf. Sec. II A). These changes are expressed by the following parameters[32]:

$$\varepsilon_1 = \left(M_1 - M_1^{\mathrm{I}}\right)/M_1, \tag{16a}$$

$$t = (A - A')/A = (B - B')/B = 1 - a, \tag{16b}$$

or

$$\varepsilon_2 = \left(M_2 - M_2^{\mathrm{I}}\right)/M_2, \tag{16c}$$

$$u = (A - A'')/A = (B - B'')/B = 1 - b, \tag{16d}$$

for impurity atom of mass $M^I{}_1$ or $M^I{}_2$ occupying either the site $\kappa = 1$ or 2, respectively. Following Vandevyver and Plumelle[32] we have considered impurity-host interaction by a single dimensionless parameter t or u, assuming that A' (or A'') and B' (or B'') are proportional to A and B, respectively. The stipulation $aA = aB$ used in Eqs. (16b) and (16d) for delineating $\overleftrightarrow{P}(\omega)$ hardly affects the high-frequency LVMs. However, by imposing this condition the perturbation matrix satisfies the rotational invariance requirement, which is explicitly invariant with respect to the translations and crystal-symmetry operations.[29]

The constructions of full-size 15×15 $\overleftrightarrow{G}^o(\omega)$ and $\overleftrightarrow{P}(\omega)$ matrices are reported in Ref. 44 for an isolated defect in zinc-blend-type semiconductors. Taking into account the symmetry of the system we have decomposed $\overleftrightarrow{G}^o(\omega)$ and $\overleftrightarrow{P}(\omega)$ into blocks corresponding to the irreducible representations of the T_d group:

$$\Gamma_{T_d} = A_1 \otimes E \otimes F_1 \otimes 3F_2. \tag{17}$$

The frequencies of local and gap modes are obtained for the light isotopic defects in different irreducible representations by solving the real part of the determinant,[44]

$$\prod_{\mu\Gamma} \det\left|\overleftrightarrow{I} - \overleftrightarrow{G}^o_{\mu\Gamma}(\omega)\,\overleftrightarrow{P}_{\mu\Gamma}(\omega)\right| = 0. \tag{18}$$

Here, $\overleftrightarrow{G}^o_{\mu\Gamma}(\omega)$ is the Green's function of the perfect crystal projected on to the defect space, and $\overleftrightarrow{P}_{\mu\Gamma}(\omega)$ is the perturbation matrix in a given irreducible representation, i.e., A_1, E, F_1, and F_2.

2. NN pair-defects: C_{3v} symmetry

The perturbation matrix $\overleftrightarrow{P}(\omega)$ for the NN pair-defect in II-VI semiconductor involves two impurity atoms occupying the sites 1 and 2 ([cf. Fig. 1(b)], respectively, causing changes in the masses at impurity sites, i.e., ε_1 [$= (M_1 - M^I{}_1)/M_1$], ε_2 [$= (M_2 - M^I{}_2)/M_2$] and the force constant variations t (i.e., 1–2, 1–3, 1–4, 1–5), u (i.e., 2–1, 2–6, 2–7, 2–8) between impurity-host atoms. An effective force constant between impurities F_{12} ($\equiv 1 - ab + \Gamma_{12} = u + t - ut + \Gamma_{12}$) is included (see Ref. 31 using Γ_{12}) to account for the changes in u, t of the isolated impurities involved in the formation of the pair-defect. The term $F_{12} < 0$ (or > 0) signifies stiffening (or softening) between the pair-bond. The point group symmetry of the defect center is C_{3v} with axis along the pair-bond involving eight atoms—causing the size of the defect space to increase to 24×24. The total representation of $\Gamma_{C_{3v}}$ reported by Ludwig[45] in the 24-dimensional space is used to block-diagonalize $\overleftrightarrow{G}^o(\omega)$ and $\overleftrightarrow{P}(\omega)$ matrices with each block along the diagonal belonging to the following irreducible representations:

$$\Gamma_{C_{3v}} = 6A_1 \otimes 2A_2 \otimes 8E. \tag{19}$$

From group-theoretical analysis[45] it is perceived that as the impurity atoms in the pair-defect remain stationary in the A_2 representation—only A_1 and E type of modes are optically active. As the degeneracies are lifted at the defect sites, one expects observing four LVM for the pair-defect with very light impurity atoms: two nondegenerate modes due to the movement of the impurity atoms along the bond [i.e., ω_1 ($A_1^+ \leftarrow\rightarrow$) and ω_4 ($A_1^- \rightarrow\rightarrow$)] and two doubly degenerate modes as a result of their vibration perpendicular to it [i.e., ω_2 ($E^+ \uparrow\downarrow$) and ω_3 ($E^- \uparrow\uparrow$)] generally with $\omega_1 > \omega_2 > \omega_3 > \omega_4$ (cf. Sec. III C1). On the other hand, only two (A_1, E) impurity modes are possible for the pair-defect involving a vacancy and a light impurity atom, e.g., O_{Te}-V_{Cd} in CdTe.

3. *Complex defects: C_s or C_{2v} symmetry*

The previous methodology of NN pair-defect is extended to define the perturbation matrix $\overleftrightarrow{P}$ for a complex center comprising three substitutional impurities [see Fig. 1(c)] occupying sites 1 (cation), 2 (anion), and 6 (cation), respectively. Following the C_{3v} case we considered the mass change parameter at impurity site 6 in terms of ε_6 [$=(M_1 - M^I{}_6)/M_1$] and the force constant variation between 6–2, 6–9, 6–10, and 6–11 impurity-host bonds by v [$=(A - A''')/A = (B - B''')/B = 1 - c$]. Similar to the NN pair-defect, an effective force constant between the impurity-atoms 2–6 ($\equiv F_{26}$) is also included. The point group symmetry for such a complex defect center is C_{2v} if $\varepsilon_1 = \varepsilon_6$, otherwise it is C_s—causing the size of the defect space to increase to 33 × 33. By constructing the total representation of $\Gamma_{C_{2v}}/\Gamma_s$ in the 33-dimensional space we have block-diagonalized $\overleftrightarrow{G}^o$ and $\overleftrightarrow{P}$ matrices belonging to the following irreducible representations[34]:

$$\Gamma_{C_{2v}} = 10A_1 \otimes 6A_2 \otimes 8B_1 \otimes 9B_2, \tag{20a}$$

and

$$\Gamma_{Cs} = 19A_1 \otimes 14A_2, \tag{20b}$$

with A_1, B_1, and B_2 (A_1 and A_2) types of vibrations being optically active. We will use this perturbation model to account for the experimental results on impurity modes of second NN pair-defects[21–24] (e.g., Al_{Zn}-Li_{Zn}; Al_{Cd}-V_{Cd}) and for analyzing the atypical FTIR data on the LVMs by complex centers involving Al donors and the intrinsic defects (see Sec. III C2) in Al-doped ZnSe and CdTe.

III. NUMERICAL COMPUTATIONS AND RESULTS

A. Lattice dynamics of Zn-Cd chalcogenides

By RIM the existing inelastic neutron scattering data of phonon dispersions[38,39] in II-VI compounds has provided us with a very good account for evaluating the interatomic interactions of host lattices (e.g., ZnS, ZnSe, ZnTe, and CdTe).[37] In cubic CdSe, the known values of first-order elastic constants, bulk modulus, and phonon frequencies at high-symmetry points from the recent *first-principles* studies[46–48] were valuable to us for constructing an optimized RIM.[49] In II-VI compounds the model has successfully explained the existing experimental data on phonon dispersions,[38,39] Debye temperatures $\Theta_D(T)$, and lattice heat capacities $C_v(T)$.[37,49] Due to a small difference in the atomic masses of Cd (112.4 amu), Te (127.6 amu), Zn (65.39 amu), and Se (78.96 amu) our RIM calculations for the density of states (DOS) in CdTe (126–135 cm^{-1}) and ZnSe (191–199 cm^{-1}) provided tiny gaps between their acoustic and optical phonon branches.[37,49] With the increase of mass difference between the cation and anion atoms, larger phonon gaps are found in the DOS for ZnS (213–277 cm^{-1}), ZnTe (150–173 cm^{-1}), and CdSe (157–175 cm^{-1}), respectively.[37,49] Consistent with the *ab initio* calculations[50] our results of the DOS have played crucial roles (cf. Sec. III B1) in identifying the specific features of defects[17–24] responsible for the observed impurity vibrational (localized and/or gap) modes in II-VI compound semiconductors.

B. Isolated defects in II-VI compounds

The impurity mode calculations reported in this section follow the procedures discussed previously.[31] In brief, the phonons (eigenvalues and eigenfunctions) of Zn-Cd chalcogenides obtained from the RIM at 64 000 $\vec{q}$ points in the Brillouin zone (cf. Sec. III A) are incorporated for computing lattice Green's functions matrix elements of the host materials by using a root-sampling technique. Impurity vibrational

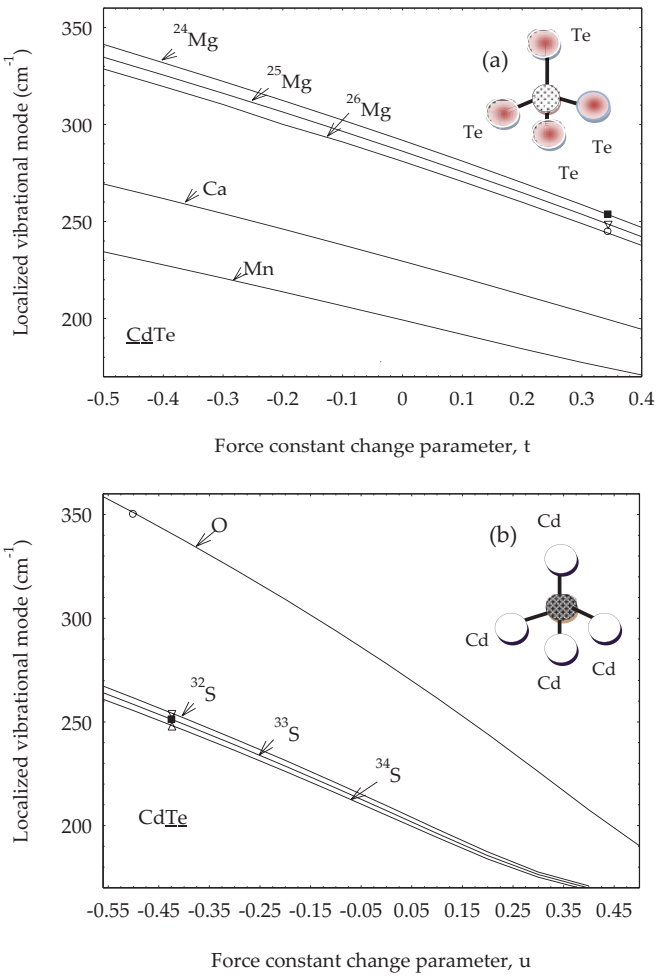

FIG. 2. (Color online) Comparison of the calculated frequencies of the F_2 localized vibrational modes in CdTe with the experimental data (□ ■∇) for defects (a) occupying Cd site versus the force constant change parameter t and (b) occupying Te site versus the force constant change parameter u.

TABLE I. Comparison of the calculated LVMs due to isolated light defects (T_d symmetry) occupying the cation and anion sites in CdTe, CdSe (cubic), ZnTe, ZnSe, and ZnS.

	Local vibrational modes (cm^{-1})			
System	Mass defect approximation	Calculated (with impurity-host interaction)	Experimental[a]	Force constant variation t, u
*Cd*Te:^{7}Li	510.00	325.0	325.0	0.910
*Cd*Te: Be	469.40	391.0	391.0	0.435
*Cd*Te:^{24}Mg	291.86	253.6	253.3	0.344
*Cd*Te:^{25}Mg	286.23	248.7	248.9	0.344
*Cd*Te:^{26}Mg	280.97	244.1	244.7	0.344
*Cd*Te:Al	275.91	299.1	299.0	− 0.230
*Cd*Te:^{40}Ca	229.58	211.1	210.6	0.210
*Cd*Te:^{42}Ca	224.72	206.9	206.8	0.210
*Cd*Te:^{44}Ca	220.04	202.6	202.8	0.210
Cd*Te*:^{16}O	278.16	350.4	350.0	− 0.500
Cd*Te*:^{32}S	209.63	254.2	254.1	− 0.424
Cd*Te*:^{33}S	207.28	251.0	250.7	− 0.424
Cd*Te*:^{34}S	205.01	248.3	247.5	− 0.424
Cd*Te*:^{31}P	212.00	319.0	322.0	− 1.10
*Cd*Se:^{24}Mg	281.23	280.4	280.9	0.010
*Cd*Se:^{25}Mg	276.90	276.0	276.2	0.010
*Cd*Se:^{26}Mg	272.85	271.50	271.9	0.010
Cd*Se*:^{32}S	282.10	264.00	264.0	0.165
Cd*Se*:^{33}S	278.22	260.74	–	0.165
Cd*Se*:^{34}S	274.52	257.32	–	0.165
*Zn*Te:Be	392.73	415.0	415.0	− 0.102
*Zn*Te:^{24}Mg	257.34	272.4	272.3	− 0.120
*Zn*Te:^{25}Mg	253.29	267.9	267.6	− 0.120
*Zn*Te:^{26}Mg	249.50	263.7	263.6	− 0.120
*Zn*Te:Al	245.90	313.1	313.0	− 0.510
*Zn*Te:^{40}Ca	296.40	240.0	240.0	− 0.282
*Zn*Te:^{42}Ca	292.42	236.0	–	− 0.282
*Zn*Te:^{44}Ca	288.63	232.3	–	− 0.282
*Zn*Te:Sr	–	218.2	218.4	− 0.710
*Zn*Te:Ba	155.30	159.2	159.2[b]	− 0.076
Zn*Te*:^{32}S	215.30	272.4	272.7	0.230
Zn*Te*:^{33}S	212.40	268.6	–	0.230
Zn*Te*:^{34}S	210.07	265.2	265.7	0.230
Zn*Te*:^{31}P	301.59	343.0	–	− 0.430
*Zn*Se:^{6}Li	531.70	410.00	411.0	0.370
*Zn*Se:^{7}Li	495.00	382.00	382.0	0.370
*Zn*Se:Be	440.80	450.00	450.0	− 0.040
*Zn*Se:^{24}Mg	293.74	305.00	305.0	− 0.080
*Zn*Se:^{25}Mg	289.50	300.70	–	− 0.080
*Zn*Se:^{26}Mg	285.60	296.5	–	− 0.080
*Zn*Se: Al	282.00	359.00	359.00	− 0.600
Zn*Se*:^{14}N	461.60	552.70	553.0	− 0.630
Zn*Se*:^{15}N	446.70	536.00	537.0	− 0.630
Zn*Se*:^{32}S	315.50	297.00	297.0	0.160
Zn*Se*:^{33}S	311.40	293.06	–	0.160
Zn*Se*:^{34}S	307.40	289.30	–	0.160
Zn*Se*:P	320.07	374.70	375.0	− 0.500
*Zn*S:Be	466.82	490.00	490.0	− 0.096
*Zn*S:^{24}Mg	360.18	380.00	380.0	− 0.200
*Zn*S:^{25}Mg	358.98	377.00	377.0	− 0.200
*Zn*S:^{26}Mg	357.60	373.90	374.0	− 0.200

TABLE I. (*Continued.*)

		Local vibrational modes (cm^{-1})		
System	Mass defect approximation	Calculated (with impurity-host interaction)	Experimental[a]	Force constant variation t, u
*Zn*S:Al	356.91	438.10	438.0	− 0.760
Zn*S*:^{76}Se	–	232.45	232.2[b]	− 0.186
Zn*S*:^{77}Se	–	231.42	231.5[b]	− 0.186
Zn*S*:^{78}Se	–	230.44	230.6[b]	− 0.186
Zn*S*:^{80}Se	–	228.52	228.5[b]	− 0.186
Zn*S*:^{82}Se	–	227.80	227.9[b]	− 0.186

[a]References 17–20.
[b]Gap mode.

modes are then determined from the solutions of Eq. (15) for various defect centers by considering appropriate perturbation matrices (cf. Sec. II D). Here we consider the following cases.

1. Single isolated defects

In CdTe the calculated results of LVMs in the triply degenerate F_2 irreducible representation are displayed in Figs. 2(a), 2(b) as a function of force constant change parameters t or u for light impurities occupying either cation or anion sites, respectively. In Table I we have compiled the experimental data of local and/or gap modes in II-VI compounds[17–24] for isolated [isoelectronic (i_{II} or i_{VI}) and charged ($d^{+}{}_{II(VI)}$ or $a^{-}{}_{II(VI)}$)] defects of T_d symmetry along with the values obtained in the mass-defect approximation (MDA). Contrary to the distinct impurity-host interactions (Table I) for various charged defects our calculations for the isotopic shifts of LVMs in Zn-Cd chalcogenides provided strong revelations of the inflexible values for each isotopic impurities, e.g., Li, (^{6}Li, ^{7}Li); N (^{14}N, ^{15}N); Mg (^{24}Mg, ^{25}Mg, ^{26}Mg); Ca (^{40}Ca, ^{42}Ca, ^{44}Ca); S (^{32}S, ^{33}S, ^{34}S); and Se (^{76}Se, ^{77}Se, ^{78}Se, ^{80}Se, ^{82}Se).[17–24]

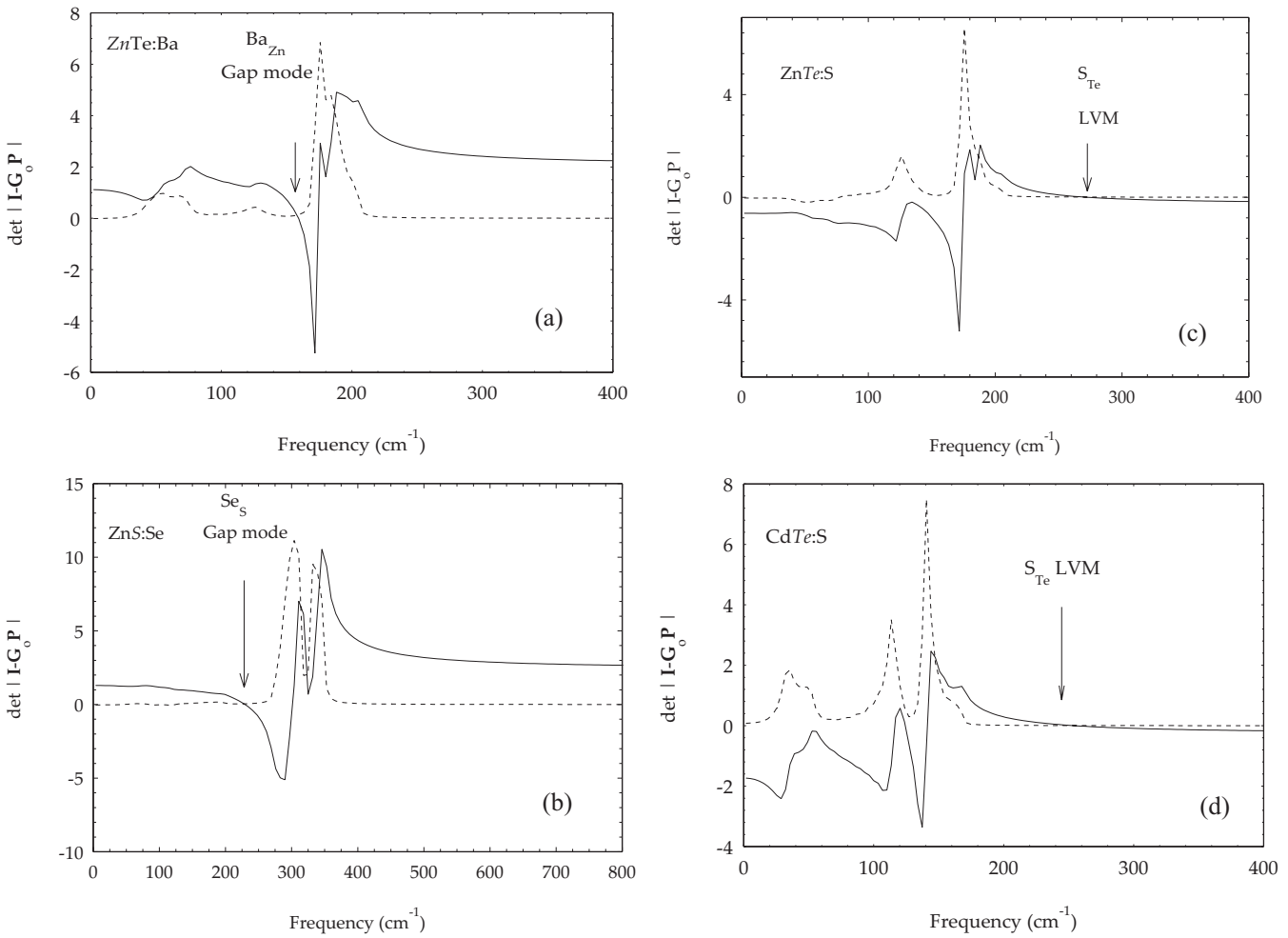

FIG. 3. Calculated real (solid line) and imaginary (dotted line) parts of the det $|\, I - G_o P \,|$ (cf. Sec. II D) in the F_2 representation showing gap modes of (a) Ba_{Zn} in *Zn*Te, (b) Se_S in Zn*S*, and the local modes of (c) S_{Te} in Zn*Te* and (d) S_{Te} in Cd*Te*.

By retaining the values of impurity-host bonding (see Table I) we have simulated the real (full lines) and imaginary (dashed lines) parts [see Figs. 3(a)–3(d)] of the $\det|\overleftrightarrow{I} - \overleftrightarrow{G}^{o}_{F2}(\omega)\ \overleftrightarrow{P}_{F2}(\omega)|$ for four isolated defects, viz. (a) Ba_{Zn} in $ZnTe$, (b) Se_S in ZnS, (c) S_{Te} in $ZnTe$, and (d) S_{Te} in $CdTe$. The crossings of the real part of the determinant through zero provide frequencies of the gap and LVM. Although the simulated results for the gap modes of Ba_{Zn} in $ZnTe$ and Se_S in ZnS [Figs. 3(a), 3(b)] as well as the local modes of S_{Te} in $ZnTe$ and $CdTe$ [Figs. 3(c), 3(d)] provide strong corroboration to the observed FTIR data,[19,20] the lattice dynamical study does not support, however, the phonon absorption bands near 106.1 and 144.6 cm^{-1} as the gap modes of S_{Te} in $CdTe$ and $ZnTe$, respectively, simply because they do not fall in the phonon gaps of the host lattice materials.

In contrast to the findings of Gaur *et al.*,[51] our results of the relative force variations in Zn-Cd chalcogenides are large even for isoelectronic impurities (see Table I) and quite appreciable for the charged defects. In III-V compounds, Bellomonte[52] argued in favor of the size effect for the large softening in $GaAs$:B based on a small Van Vechten–Phillips[53] radius of B (0.853 Å) compared to the replaced Ga (1.225 Å) atom. Although we did find an appreciable softening for B in GaP and $GaAs$, stiffening was noted, however, for B in InP.[31] Further evidence in II-VI materials that the size of substitutional atoms does not reflect the NN bond strength (see Table I) can be found from the diverse values obtained for the isoelectronic S in $CdSe$ and $CdTe$ in which both Se (1.225 Å) and Te (1.405 Å) atoms have radii larger than S (1.127 Å).

2. *Unique force variations*

In Zn-Cd chalcogenides the signs of t or u for various isolated defects (see Table I) find no correlation between the sizes of impurity host atoms. Here we have proposed simple empirical relationships providing corrections to the force constants for the closest mass isoelectronic defects and impurities carrying static charges. For instance, the values of Δt estimated for an isoelectronic $\{\mathrm{Mg}\ (i)\}$ and a donor $\{\mathrm{Al}\ (d^{+})\}$ or an isoelectronic $\{\mathrm{Be}\ (i)\}$ and an acceptor $\{\mathrm{Li}\ (a^{-})\}$ substituting on the *cation* sites exhibit the following trends:

$$\Delta t\ \{a^{-}_{\mathrm{II}} - i_{\mathrm{II}}\} > 0 \quad \text{softening}, \tag{21a}$$

$$\Delta t\ \{d^{+}_{\mathrm{II}} - i_{\mathrm{II}}\} < 0 \quad \text{stiffening}. \tag{21b}$$

Similarly, the values of Δu obtained from the limited impurity mode data available for a closest mass isoelectronic $\{\mathrm{S}\ (i)\}$ and an acceptor $\{\mathrm{P}\ (a^{-})\}$ occupying the *anion* site reveals

$$\Delta u\ \{a^{-}_{\mathrm{VI}} - i_{\mathrm{VI}}\} < 0 \quad \text{stiffening}, \tag{21c}$$

and we expect

$$\Delta u\ \{d^{+}_{\mathrm{VI}} - i_{\mathrm{VI}}\} > 0 \quad \text{softening}, \tag{21d}$$

for an isoelectronic $\{\mathrm{S}\ (i)\}$ and a donor $\{\mathrm{Cl}\ (d^{+})\}$ occupying the *anion* site in II-VI materials. The absolute values of the relative variations in Δt and Δu for single charge (a^{-}, d^{+}) and isolectronic (i) defects producing LVMs in II-VI compounds are seen to lie well within 40–70%. Although these correlations are found independent of the long-range Coulomb forces, we strongly argue that the charged impurities in compound semiconductors affect only the short-range forces via the redistribution of the electron-charge density. Our arguments find support from a self-consistent super-cell study by Baraff *et al.*,[54] where the electronic-charge density contours are simulated for both the perfect GaP and imperfect GaP:O systems to mark the evidence of a weak bonding between the O_P–Ga bonds. We believe that these unique trends in force variations are significant to serve as a good starting point to analyze the existing[21–24] FTIR and Raman scattering[19] data on impurity modes of various complex centers [e.g., C_{3v}: (Al-P), (Ga-P), (In-P); C_s: (Al-Li), etc.; see Sec. III C1] in Zn-Cd chalcogenides. After estimating the force variations for several isolated charged defects, e.g., O_{Te}, P_{Te} in $CdTe$, $ZnTe$; Ga_{Cd}, Al_{Cd} in $CdTe$, Al_{Zn}; Ga_{Zn} in $ZnSe$, we have examined (cf. Sec. III C2) the spectroscopic data of complex centers in II-VI compounds.

C. Complex defects in II-VI compounds

By using the methodology outlined in Sec. II D we now investigate the impurity vibrational modes of various complex defect centers of C_{3v} and C_s/C_{2v} point group symmetries in II-VI semiconductors. Here we consider the following cases.

1. *NN donor-acceptor pairs*

In II-VI compounds the presence of Al or P impurities have the tendency to form complex centers with native defects making the analyses of infrared absorption spectra on local modes very difficult. However, the use of counter doping (e.g., ZnSe:Al with Li, Cu, Ag, Au and CdTe:P with Al, Ga, In) has always been helpful in discriminating LVMs providing valuable information of the defect-pairing processes. Despite many successes there have been consistent problems for the interpretation of infrared spectra especially when the number of local mode frequencies is larger or smaller than expected from the complex-defect symmetry.[21–25] Here we present a systematic study using Green's function method of calculating the local modes for NN pair-defects (C_{3v} symmetry) in double-doped II-VI compounds and analyze the results by comparing them with the experimental data. Similar calculations of second NN pair-defects (C_s symmetry) in ZnSe:Al (CdTe:Al) samples counter doped with Li will be presented in Sec. III C2.

In CdTe the Al_{Cd}–P_{Te} (say) pair-defect is envisioned [see Fig. 1(b)] forming a NN complex between an Al atom occupying the Cd-site (Al_{Cd}: donor) and a P atom substituting for the NN Te-site (P_{Te}: acceptor). Green's function theory in the MDA has offered LVMs of P_{Te} (∼212.0 cm^{-1}) and Al_{Cd} (∼275.91 cm^{-1}) much lower than the observed ω_{LVMs} ∼322 cm^{-1}, 299 cm^{-1}, respectively, requiring large stiffening in the P_{Te}-Cd and Al_{Cd}-Te bonds. In this defect center of C_{3v} symmetry with trigonal ⟨111⟩ axis along the pair-bond, one expects splitting of the two triply degenerate F_2 local modes of isolated Al_{Cd} and P_{Te} defects into four impurity modes—two doubly degenerate E and two nondegenerate A_1 modes. In Fig. 4(a) the results of our calculations are displayed for the LVMs of Al_{Cd} donor paired with other impurities in CdTe occupying the NN Te-site. Clearly, the simulation revealed the possibility of four modes when Al_{Cd} is coupled with impurities having much lighter masses. Among these modes, two are longitudinal and nondegenerate, while the other two

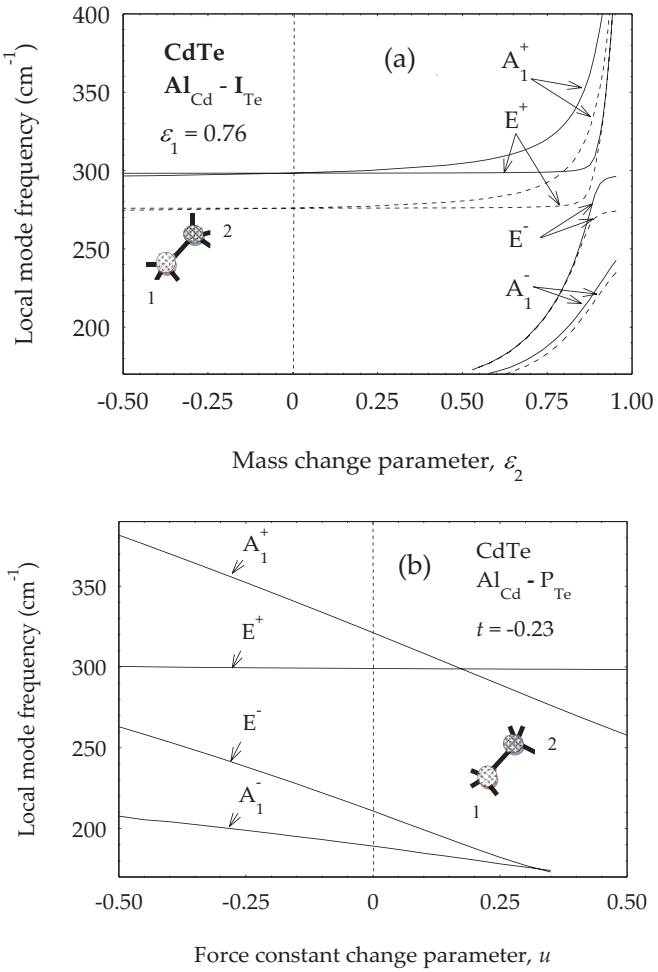

FIG. 4. (Color online) Green's function calculation of (a) the variation of localized vibrational modes as a function of ε_2 for Al_{Cd}, paired with other impurities on Te-site in CdTe; dotted lines, MDA; full lines with $t = -0.23$ (see text). (b) The variation of localized vibrational modes as a function of u for Al_{Cd}-P_{Te} pair keeping $t = -0.23$.

are transverse and doubly degenerate. If the impurity mass occupying Te-site becomes heavier (i.e., $M^I_{Te} > 55$ amu), the antisymmetric modes fall into the band continuum, and we expect only two symmetric modes. As anticipated for $\varepsilon_2 = 0$, $A_1^+ = E^+$ provides the LVM frequency of an isolated Al_{Cd} donor in CdTe.

By retaining the value ($t = -0.23$) of an isolated Al_{Cd} case we report in Fig. 4(b) the effects of u on the impurity modes of Al_{Cd}–P_{Te} pair-defect in CdTe. Some of the salient features shown in Fig. 4(b) are summarized here. For example, (a) the frequency of E^+ mode does not appreciably change with the variation of u; it varies considerably (not shown here), however, with the alteration of t and/or F_{12}. (b) For $u > 0.25$ the A_1^+ mode attains frequency lower than the E^+ mode—the *two* antisymmetric modes disappear and fall into the band continuum if the value of u further increases (please note that $u = 1.0$ would represent an ideal Al_{Cd}–V_{Te} NN pair where Al-donor forms a defect center with Te-vacancy). (c) All four LVMs of the Al_{Cd}–P_{Te} pair in CdTe require a large stiffening in the force constant u (i.e., $u < -0.25$). These observations are quite significant and have played important roles in analyzing the limited experimental data available for the impurity vibrational modes of NN pairs in II-VI compound semiconductors (e.g., In_{II}-P_{VI}, Ga_{II}-P_{VI}, Al_{II}-Sb_{VI}).[23,24]

It is to be noted that our calculation in the MDA provides no impurity mode for isolated In_{Cd}; it suggests only an in-band mode for Ga_{Cd} at ∼165.2 cm^{-1} and predicts a local mode for Al_{Cd} at ∼275.91 cm^{-1}. For the double-doped CdTe:In, P system, although the substitution of In for Cd in the In_{Cd}-P_{Te} pair causes no significant size or mass change,[53] we do expect, however, force constant changes in the In_{Cd}-Te as well as between the In_{Cd}-P_{Te} bonds through the electronic charge redistribution (cf. Sec. III B2) mechanisms. With a set of values t, u, and F_{12} our Green's function calculation in CdTe for the In_{Cd}-P_{Te} pair-defect (see Table II) provided $E^+ \sim 331$ cm^{-1} and $A_1^+ \sim 304$ cm^{-1} modes, in excellent agreement with the experimental data.[23]

In the CdTe:Ga, P system besides P-related modes (269, 308, and 322 cm^{-1}), three additional absorption bands associated with the Ga-P pair are observed near 301.5, 352.5, and 357.5 cm^{-1}.[23] One must note that the mode at 352.5 cm^{-1} appeared as a shoulder to the 357.5 cm^{-1} band. Again, as compared to In, the lighter Ga atom having smaller covalent radii than the Cd atom[53] is expected to cause larger stiffening in the Ga_{Cd}-Te bonds. It is worth pointing out that there are two naturally occurring Ga isotopes [^{69}Ga (60.4%) and ^{71}Ga (39.6%)], which can form $^{69}Ga_{Cd}$-P_{Te} and $^{71}Ga_{Cd}$-P_{Te} pairs of C_{3v} point group symmetry. By using a set of force constants, our Green's function theory has provided three $A_1^+ \sim 355.14$ cm^{-1} (∼353.0 cm^{-1}) and $E^+ \sim 301.7$ cm^{-1} (unchanged) modes for the isotopic $^{69}Ga_{Cd}$($^{71}Ga_{Cd}$)-P_{Te} pair centers, in very good agreement with the observed infrared absorption bands.[23] Moreover, the calculated local mode frequencies of the pair-defects In_{Cd}-P_{Te} and $^{69}Ga_{Cd}$($^{71}Ga_{Cd}$)-P_{Te} involving one light impurity atom (P_{Te}) satisfied a simple perturbation relation[24] $\omega_{F_2}(T_d) = \sqrt{\frac{1}{3}\sum_{i=1}^{3}\omega_i^2}$ connecting the split LVMs to the isolated triply degenerate impurity mode frequency of the light impurity. Clearly, this condition for In_{Cd}-P_{Te} and $^{69}Ga_{Cd}$(71Ga_{Cd})-P_{Te} pairs provided the values $\omega \sim 322$ and 321 (320 cm^{-1}) in very good accord with the F_2 mode frequency of P_{Te} (T_d) 322 cm^{-1}.

Despite theoretical predictions no local modes related to the Al-P pair vibrations are observed for the double-doped CdTe:Al, P system. In the infrared absorption measurements[23] besides the three P-related bands, the only extra mode seen at 302 cm^{-1} is assumed to be the Al_{Cd} (T_d) ω_{LVM} 299 cm^{-1}. It is likely that the shift of this mode frequency by a few wave numbers is caused by the high dopant concentrations. In the as-grown CdTe:Al samples the observation of LVMs for Al_{Cd}-V_{Cd} complex center (C_s-symmetry) by infrared studies[23] has suggested the compensation of Al_{Cd} donors by the native acceptors V_{Cd}. In CdTe:Al, P (Sb)[23,24] the reason for not detecting the Al_{Cd}-V_{Cd} modes is probably related to the presence of P_{Te} (Sb_{Te}) acceptors, which limits the need of V_{Cd} to form donor-vacancy centers. Again, our Green's function theory in double-doped systems (CdTe:P, In, Ga, Al and CdTe:Al, Sb) provided strong support for the formation of In-P, Ga-P, and Al-Sb pairs involving a lighter and a heavier donor/acceptor impurity atoms. Clearly the impurity modes are expected for the lighter Al-P NN pair—the reason for not

TABLE II. Comparison of the calculated localized vibrational modes with the experimental data for NN pair-defects (C_{3v} symmetry) in CdTe.

System		Experimental[a]	Calculated LVMs (cm^{-1})		Force constant	$\omega(T_d) = \sqrt{\frac{1}{3}\sum_{i=1}^{3}\omega_i^2}$
symmetry		LVMs(cm^{-1})			parameters[d] t, F_{12}, u	
CdTe	↓					
			$^{69}Ga_{Cd}$-P_{Te}			321
		357.5	355.14	A_1		
Ga_{Cd}-P_{Te}	C_{3v}	352.5	301.7	E	− 0.14	
		301.5			− 1.476	
			$^{71}Ga_{Cd}$-P_{Te}		− 0.90	320
			353.0	A_1		
			301.7	E		
In_{Cd}-P_{Te}	C_{3v}	331.5	330.8	E	0.2	322
		305.0	303.6	A_1	− 0.808	
					− 1.26	
Al_{Cd}-Sb_{Te}	C_{3v}	334[b]	333	A_1	− 0.15	298
		279	279	E	− 0.76	
					− 0.03	
V_{Cd}-O_{Te}	C_{3v}	1108[c]	212	A_1	1.0	347
		1097	397	E	1.0	
					− 0.84	

[a]Reference 23.
[b]Reference 24.
[c]Reference 17.
[d]See text.

observing them by infrared spectroscopy is not understood, although it may be related to the fact that both Al and P in CdTe independently required large stiffening (cf. Table I) in the force constants.[24]

2. *Second NN defects in II-VI compounds*

Despite extensive PL studies in Al-doped II-VI materials, the role of native defects as activators and impurities as coactivators has not been completely explicable.[55–57] In many luminescence studies, although different defect models for active centers are proposed, the identification of their microscopic structures remains contentious.[58] While the infrared absorption studies of LVMs in CdTe:Al supported the self-compensation mechanism (i.e., the formation of cation vacancies V_{Cd} leading to Al_{Cd}-V_{Cd} centers), the results of impurity modes in ZnSe:Al are rather atypical and cannot be interpreted in terms of a similar Al_{Zn}-V_{Zn} defect.[24] On the other hand, when Li, Ga, Cu, Ag, or Au was introduced into CdTe:Al and ZnSe:Al as a second impurity the two systems revealed a great deal of similarity. For the *X* center in ZnSe:Al an antisite defect ($2Al_{Zn}$-Zn_{Se}) that we have evaluated is probably the best possible complex center, which explains the experimental results on LVMs and is theoretically justified.

To comprehend the infrared absorption features of a second NN pair-defect [$^6Li_{Cd}$-Al_{Cd} in CdTe (say)], we have displayed in Fig. 5 the results of our calculated LVMs as a function of *t* (i.e., the impurity-host interaction between $^6Li_{Cd}$-Te bonds) while keeping the interaction *v* unchanged for Al_{Cd} (T_d). Since the triple degeneracy of the F_2 modes are lifted at the defect sites, our Green's function simulations revealed six local modes for the pair $^6Li_{Cd}$-Al_{Cd} defect having two light impurity atoms occupying the second NN Cd sites in CdTe. Among the three impurity modes associated with the vibrations of $^6Li_{Cd}$, two of the A_1 mode frequencies decrease with the softening between $^6Li_{Cd}$-Te bonds (see Fig. 5), while the vibrational modes linked to Al_{Cd} are not affected. Again, the changes (not shown here) in the force constants F_{12}, F_{26}, and *v* (between Al_{Cd}-Te) can, however, modify all the six local-mode frequencies. By using an appropriate set of force constants based on the correlation of ionicity/covalency with bond strength, the calculated results for the LVMs of several pair-defects in CdTe and ZnSe reported in Table III are compared with the existing experimental data.[21–24]

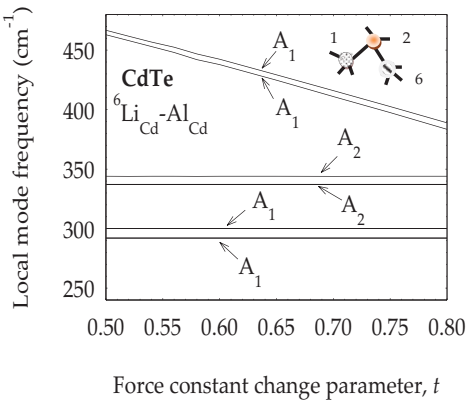

FIG. 5. (Color online) Green's function calculation for the variation of localized vibrational modes as a function of *t* (see text) for $^6Li_{Cd}$-Al_{Cd} second NN pair (with $v = -0.23$) in CdTe.

TABLE III. Comparison of the calculated localized vibrational modes with the experimental data for defects of C_s/C_{2v} symmetry in CdTe and ZnSe.

System symmetry		Experimental LVMs (cm^{-1}) ω_i, A_{II}-B_{II}	Calculated LVMs (cm^{-1}) I		II		Force constant parameters[d] t, F_{12}, F_{26}, v I	II	$\omega_{A_{II}}(T_d)$	$\omega_{B_{II}}(T_d)$[e]
CdTe[a]	↓									
Al_{Cd}-V_{Cd}	C_s	326	326	A_1			−0.12		300	
		287	288	A_1			−0.68			
		282	287	A_2			1.0			
							1.0			
$^7Li_{Cd}$-Al_{Cd}	C_s	332	332.7	A_1			0.9		325	299.5
		325	326.1	A_2			0.92			
		318	319	A_1			−0.51			
		...	307.1	A_2			–0.23			
		299	298.2	A_1						
		292.5	293.1	A_1						
$^6Li_{Cd}$-Al_{Cd}	C_s	355	354.2	A_1			0.9		345	300
		349.5	350.1	A_2			0.92			
		328	330.0	A_1			−0.51			
		311	309.3	A_2			−0.23			
		299	298.3	A_1						
		292.5	293.1	A_1						
ZnSe[b]	↓									
Al_{Cd}-V_{Cd}	C_s		388	A_1			−0.49		360	
			346	A_1			−0.92			
			344	A_1			1.0			
							1.0			
$^7Li_{Zn}$-Al_{Zn}	C_s	392	393	A_1			0.345		383	358
		382	382	A_2			0.495			
		...	376	A_1			−0.75			
		359	367	A_2			−0.67			
		356	358	A_1						
		350	348	A_1						
$^6Li_{Zn}$-Al_{Zn}	C_s	420.5	420	A_1			0.345		408	359
		410.5	411	A_2			0.495			
		389	392	A_1			−0.75			
		373	372	A_2			−0.67			
		359	358	A_1						
		350	348	A_1						
Al	(X center)[c]		Al_{Zn}-Al_{Zn}		Al_{Zn}-Zn_{Se}-Al_{Zn}					
		392.93	393.3	A_1	394.02	A_1				
		388.22	388.73	B_1	389.05	B_1	−0.463	−0.471		
		346.24	346.01	B_2	346.64	B_2	0.972	0.981		
		345.06	...		...		0.972	0.981		
		343.01	342.84	B_1	344.02	B_1	−0.463	−0.471		
		341.48	...		...					
		338.81	339.94	A_1	338.50	A_1				
		337.15	337.95	B_2	337.43	B_2				

[a]References 21 and 22.
[b]Reference 23.
[c]References 21 and 24.
[d]Reference 31.
[e]$\omega_{B_{II}}(T_d) = \sqrt{\frac{1}{3}\sum_{i=1}^{6}[\omega_i^2 A_{II} - B_{II}] - \omega_{A_{II}}^2}$.

Again, the main purpose of using Li as a compensating species in CdTe:Al and ZnSe:Al systems was to help interpret the Al-related LVM.[21,22] Despite extensive studies of impurity-induced absorption bands related to the pair-defects, there have been difficulties in the interpretations of data because of the smaller number of modes observed than expected theoretically.[21,22,59,60] In the ZnSe:^{6}Li, Al sample, for instance, a prominent mode near 420.5 cm^{-1} was suggested earlier[59] but not detected due to its overlap with a strong two-phonon lattice absorption band. Now the emergence of a sharp absorption line of an isotopic counterpart at 392 cm^{-1} in ZnSe:^{7}Li, Al[21] has made it clear that there has to be an impurity mode near ∼420.5 cm^{-1} for ZnSe:^{6}Li, Al, and it cannot be related to an impurity-induced enhancement of ZnSe two-phonon lattice band. A close inspection of the infrared absorption results reveals that the CdTe:^{6}Li, Al system has impurity mode features similar to those of ZnSe:^{6}Li, Al. Our results of LVMs using Green's function theory with a set of force constants for $^6\mathrm{Li_{II}} + \mathrm{Al_{II}}$ provided reasonably accurate isotopic shifts of impurity modes as well as the missing data associated with $^7\mathrm{Li_{II}}$-$\mathrm{Al_{II}}$ pairs. Consistent with experimental observations, our calculations for the two lowest frequency bands show no shift. Again from the similarity of force constants, the agreement that we achieved for LVMs in the two material systems support our assertion that the observed absorption spectra[21] are related to the vibrations of $\mathrm{Li_{Zn(Cd)}}$–$\mathrm{Al_{Zn(Cd)}}$ pairs in which Li acts as a compensating acceptor $\mathrm{Li_{Zn(Cd)}}$ and is located on a second NN site of the $\mathrm{Al_{Zn(Cd)}}$ donor in ZnSe and CdTe. To check the validity of our results a simple perturbation relationship (i.e., $\omega^2_{A_{II}} + \omega^2_{B_{II}} = \frac{1}{3}\sum_{i=1}^{6}[\omega_i^2, A_{II} - B_{II}]$) is applied to the pair centers (C_s-symmetry) in II-VI compounds having two weakly coupled impurities, where ω_i, $A_{II} - B_{II}$ represent the calculated LVMs of the defect-pair and $\omega_{A_{II}}, \omega_{B_{II}}$ are the local modes associated with isolated A_{II} and B_{II} defects, each of T_d symmetry. In Table III we summarized the outcome of the relationship for various defect pairs in CdTe and ZnSe.

Next we report our attempt to identify the unusual number of LVMs in ZnSe:Al (X center). From the observed absorption bands (see Table III) one may envisage that either there is more than one Al per defect or that there is more than one type of Al defect. The analysis of impurity vibrations in ZnSe for both isolated and pair-defects have confirmed the local mode of $\mathrm{Al_{Zn}}$ at 359 cm^{-1}. Among other models a NN $\mathrm{Al_{Zn}}$-$\mathrm{Al_{Se}}$ (C_{3v} symmetry) pair involving two Al atoms each sitting on Zn and Se sites is unlikely to explain the large number of LVM absorption features observed for the X center. Our Green's function calculation for the $\mathrm{Al_{Zn}}$-$\mathrm{Al_{Se}}$ pair-defect in the MDA has suggested four impurity modes near ∼348 (A_1^+), 332 (E^+), 292 (E^-), and 254 (A_1^-) cm^{-1}. Clearly, the A_1^- mode is anticipated in the region where the phonon absorption in ZnSe will interfere with the observation. Moreover, the number of LVMs for this NN pair center with a reasonable set of perturbation parameters (t, u, F_{12}) is insufficient to account for the number of modes observed—consequently the model $\mathrm{Al_{Zn}}$-$\mathrm{Al_{Se}}$ cannot be ascribed to the origin of the infrared absorption features. Another possibility suggested previously, to assess the origin of LVMs for the X center, is a well-known luminescence center, i.e., $\mathrm{Al_{Zn}}$-$\mathrm{V_{Zn}}$ (C_s symmetry). Once again, our Green's function calculations for the center $\mathrm{Al_{Zn}}$-$\mathrm{V_{Zn}}$ providing three nondegenerate modes (see Table III) at 388, 346, and 344 cm^{-1} has not successfully accounted for the number of observed LVMs. There are several other possible configurations involving multiple Al, which may provide a sufficient number of absorption bands not considering the accidental degeneracies to account for the observed absorption features. The most appealing of these are (a) $\mathrm{Al_{Zn}}$-$\mathrm{Al_{Zn}}$:C_{2h} symmetry and (b) $\mathrm{Al_{Zn}}$-$\mathrm{Zn_{Se}}$-$\mathrm{Al_{Zn}}$:C_{2v} symmetry.

Based on the Green's function simulations, we find that most but not all of the remaining LVMs (see Table III, set I) arise from a center involving two $\mathrm{Al_{Zn}}$ (i.e., $\mathrm{Al_{Zn}}$-$\mathrm{Al_{Zn}}$:C_{2h} symmetry) defects occupying the second NN Zn-sites, as evidenced by comparison with the experimental results. It is to be noted that the same level of conformity is achieved (see Table III, set II) if a $\mathrm{Zn_{Se}}$ antisite defect is included in the center (i.e., $\mathrm{Al_{Zn}}$-$\mathrm{Zn_{Se}}$-$\mathrm{Al_{Zn}}$:C_{2v} symmetry). We are not successful, however, when a Zn vacancy is involved ($\mathrm{Al_{Zn}}$-$\mathrm{V_{Zn}}$-$\mathrm{Al_{Zn}}$). Although the existence of antisite-type defects proposed here has not been well established, they have been predicted and suggested as possible explanations of the experimental data.[25] The perusal of Table III reveals that two absorption bands occurring at 345.06 and 341.48 cm^{-1} are not explained either by the $\mathrm{Al_{Zn}}$-$\mathrm{Al_{Zn}}$ pair or by antisite defect models. Although difficult to conclusively identify these lines, it is speculated, however, that the values (see Table III) for the LVMs arising from $\mathrm{Al_{Zn}}$-$\mathrm{V_{Zn}}$ at 344, 346, and 388 cm^{-1} that we calculated may correspond to the observed bands at 341.48, 345.06, and 388.22 cm^{-1}, respectively. As the 388.22 cm^{-1} band is anomalously broad it is likely that the mode may have two unresolved LVMs arising from both the antisite and vacancy defect models. The dimer center ($2\mathrm{Al_{Zn}}$-$\mathrm{V_{Zn}}$) proposed earlier[55–57] to explain the electrical compensation at high Al by a native defect provided the necessary binding energy to make the complex stable—it is to be noted that the requirement by an antisite model is equally satisfied. Furthermore, the heavily Al-doped ZnSe, ZnTe, and ZnS are observed to have an analogous structure, all arising from presumably the same complex involving Al. Electron-spin resonance on ZnTe:Al show that while $\mathrm{Al_{Zn}}$-$\mathrm{V_{Zn}}$ type complexes occur in this material, the concentrations are much too small to account for the amount of compensation observed.[55–57] Due to the similarity of infrared absorption in ZnTe, a complex involving $\mathrm{Zn_{Se}}$ antisites instead of $\mathrm{V_{Zn}}$ could provide the necessary compensation without having to invoke unrealistic $\mathrm{V_{Zn}}$ concentrations. As the recombination mechanism for PL in ZnSe:Al is found to involve an extended donor/acceptor pair in lightly doped material and a relatively close donor/acceptor pair in heavily doped material, such an interpretation is coherent with the acceptor being either $\mathrm{V_{Zn}}$ or $\mathrm{Zn_{Se}}$ and, therefore, cannot provide a firm distinction between them. Thus, an antisite complex model ($\mathrm{Al_{Zn}}$-$\mathrm{Zn_{Se}}$-$\mathrm{Al_{Zn}}$) for the X center is consistent with all the experimental observations and is theoretically justified as well—making it the more likely identity for the native defect compensating neighboring $\mathrm{Al_{Zn}}$ donors in ZnSe.

IV. SUMMARY AND CONCLUSIONS

By using a realistic lattice dynamical approach in the Green's functions framework we have reported the vibrational properties of defects in tetrahedrally coordinated II-VI

compound semiconductors. Our RIM calculations of phonon dispersions[37] for ZnS, ZnSe, ZnTe, and CdTe compared well with the inelastic neutron scattering data,[38,39] while the lattice dynamics of cubic CdSe is optimized[49] with the inputs of various materials properties from the first-principles calculations.[46–48] The DOS for Cd-Zn chalcogenides providing prominent features in the phonon spectrum played crucial roles for elucidating the dynamical and thermal properties, while the simulations of Green's functions of the perfect and imperfect crystals helped explicate impurity modes for isolated defects and defects in complex configurations. The study of LVMs (see Table I) for many isolated substitutional defects occupying either cation or anion sites has provided distinct variations of t or u—revealing a moderate value for the isoelectronic and a higher value for the charged (d^+, a^-) defects. Consistent with experiments, the isotopic shift of ω_{LVM} has offered strong revelation for the inflexible impurity-host interactions. No correlation is found between the signs of t or u and the size of impurity-host atoms. A unique force-variation correlation is proposed offering corrections to the NN force constants between the closest mass isoelectronic and impurities carrying static charges on the cation and/or anion sites. This articulation has played an important role in defining $\overleftrightarrow{P}(\omega)$ and in analyzing the infrared absorption data on impurity modes confirming the formation of $\mathrm{In(Ga)_{II}}$-$\mathrm{P_{VI}}$ NN donor-acceptor pairs. In corroboration with the experimental results, our study of LVMs in Li-doped CdTe:Al (ZnSe:Al) has clearly established the second NN $\mathrm{Li_{Cd(Zn)}}$-$\mathrm{Al_{Cd(Zn)}}$ pairs indicating the passivation of group-I acceptors via the interaction with group-III elements acting as donors. Our proposal of an antisite defect model $\mathrm{Al_{Zn}}$-$\mathrm{Zn_{Se}}$-$\mathrm{Al_{Zn}}$ for the X center is consistent with the existing infrared absorption data and is equally justified by theoretical considerations making it the more likely identity for the native defect compensating neighboring $\mathrm{Al_{Zn}}$ donors in ZnSe.

ACKNOWLEDGMENTS

D.N.T. acknowledges useful discussions on the subject matter with M. D. Tiwari of Indian Institute of Information Technology, Allahabad, India and for the Innovation Grant that he received from the School of Graduate Studies at Indiana University of Pennsylvania, Indiana, Pennsylvania. The work of Z.C.F. at the National Taiwan University was supported by Grants No. NSC 98-2221-E-002-015-MY3 and No. NSC 98-3114-E-005-002-CC2 and by NTU Excellent Research Project (10R80908). T.R.Y. at the National Taiwan Normal University was supported by Grants No. NSC 100-3113-S-003-004 and No. NSC 100-3113-S-003-015.

*talwar@iup.edu, fengzc@cc.ee.ntu.edu.tw, yang1@ntnu.edu.tw

[1] S. Adachi, *Properties of Semiconductor Alloys,* Wiley Series in Materials for Electronic and Optoelectronic Applications (Wiley, 2009).

[2] G. E. Hallani, A. Ryah, N. Hassanain, M. Loghmarti, A. Mzerd, A. Arbaoui, N. Achargui, Y. Laaziz, N. Chahboun, and E. K. Hlil, *Progress in Electromagnetics Research Symposium, Marrakesh, Morocco* (Mar. 20–23, 2011), p. 1897 [www.piers.org].

[3] H. Qiao, B. Guan, T. Böcking, M. Gal, J. J. Gooding, and P. J. Reece, Appl. Phys. Lett. **96**, 161106 (2010).

[4] T. Park, J. Lee, W. Lee, J. Ahn, and W. Yi, in *22nd Intl. Vacuum Nanoelectronics Conference*, Shizuoka, Japan, 2009, p. 275.

[5] W. J. Min, J. Sunghan, J. L. Sung, K. Yongwook, and S. S. Koo, J. Phys. Chem. A **113**, 9588 (2009).

[6] C. Reig, M.-D. Cubells-Beltrán, and D. Ramírez Muñoz, Sensors **9**, 7919 (2009).

[7] M. B. Reine, *Proc. SPIE*, Vol. 72982 (Orlando, Florida, May 7, 2009).

[8] M. M. Crouse, T. L. James, and D. Crouse, in *SPIE Proceedings Nanophotonics and Macrophotonics for Space Environments II*, Vol. 70950, edited by E. W. Taylor and D. A. Cardimona (August 26, 2008).

[9] P. V. Kamat, J. Phys. Chem. C **112**, 18737 (2008).

[10] C. Reig, C. Gómez-García, and Sanjosé V. Muñoz, J. Microelectronics **38**, 327 (2007).

[11] A. Rogalski, Opto-Electronics Review **14**, 87 (2006).

[12] M. C. Gupta and J. Ballato, Eds., *Handbook of Photonics* (Taylor & Francis, New York, 2006).

[13] S. K. Shin, H.-J. Yoon, Y. J. Jung, and J. W. Park, Curr. Opin. Chem. Biol. **10**, 423 (2006).

[14] P. Swaminathan, V. N. Antonov, J. A. N. T. Soares, J. S. Palmer, and J. H. Weaver, Phys. Rev. B **73**, 125430 (2006).

[15] S. Stepanov, in *Handbook for Advanced Electronic and Photonic Materials and Devices,* edited by H. S. Nalwa, Vol. 2 (Academic Press, San Diego, 2001), p. 205.

[16] M. C. Tamargo, Ed., *II-VI Semiconductor Materials and Their Applications: Optoelectronic Properties of Semiconductors and Superlattices*, Vol. 12 (Taylor & Francis, New York, 2001).

[17] G. Chen, I. Mitkowski, S. Rodriguez, and A. K. Ramdas, Phys. Rev. Lett. **96**, 035508 (2006); G. Chen, I. Mitkowski, S. Rodriguez, and A. K. Ramdas, Phys. Rev. B **75**, 125204 (2006).

[18] H. J. Stein, Appl. Phys. Lett. **64**, 1520 (1994).

[19] E. Oh, C. Parks, I. Miotkowski, M. D. Sciacca, A. J. Mayur, and A. K. Ramdas, Phys. Rev. B **48**, 15040 (1993).

[20] M. D. Sciacca, A. J. Mayur, N. Shin, I. Miotkowski, A. K. Ramdas, and S. Rodriguez, Phys. Rev. B **51**, 6971 (1995); M. Dean Sciacca, A. J. Mayur, H. Kim, I. Miotkowski, A. K. Ramdas, and S. Rodriguez, *ibid.* **53**, 12878 (1996); M. J. Seong, I. Miotkowski, and A. K. Ramdas, *ibid.* **59**, 12911 (1999).

[21] J. S. Ko and W. G. Spitzer, J. Phys. C: Solid State Phys. **15**, 5593 (1982); J. Appl. Phys. **53**, 3894 (1982); W. M. Theis, D. N. Talwar, M. Vandevyver, and W. G. Spitzer, *ibid.* **58**, 2553 (1985).

[22] A. Krol, M. J. Kozielski, and W. Nazarewicz, Phys. Status Solidi B **90**, 649 (1978).

[23] B. V. Dutt and W. G. Spitzer, J. Appl. Phys. **48**, 2107 (1977); **48**, 954 (1977).

[24] W. G. Spitzer, *Advances in Solid State Physics*, edited by O. Madelung (Pergamon Press, Oxford, 1971), vol. XI, p. 1; B. V. Dutt and W. G. Spitzer, J. Appl. Phys. **47**, 573 (1976); B. V. Dutt, M. Al-Delaimi, and W. G. Spitzer, *ibid.* **47**, 565 (1976).

[25] R. C. Newman, *Infrared Studies of Crystal Defects* (Barnes and Noble, New York, 1972); R. C. Newman, in *Semiconductors and Semimetals*, edited by E. Weber (Academic, New York, 1993), vol. 38, Chap. 4.

[26]S. W. Biernacki, U. Scherz, and Ch. Schrepel, Phys. Rev. B **56**, 4592 (1997).
[27]L. Zhang, J. T-Thienprasert, M.-H. Du, D. J. Singh, and S. Limpijumnong, Phys. Rev. Lett. **102**, 209601 (2009); J. T-Thienprasert, S. Limpijumnong, A. Janotti, C. G. Van de Waal, L. Zhang, M.-H. Du, and D. J. Singh, Comp. Mat. Sci. **49**, S245 (2010).
[28]K. Kunc, Ann. Phys. (Paris) **8**, 319 (1973-74).
[29]A. A. Maradudin, E. W. Montroll, G. H. Weiss, and I. P. Ipatova, in *Solid State Physics*, 2nd ed., edited by F. Seitz, D. Turnbull, and H. Ehrenreich (Academic, New York, 1971).
[30]R. J. Elliott, J. A. Krumhansl, and P. L. Leath, Rev. Mod. Phys. **46**, 465 (1974).
[31]D. N. Talwar in *Dilute III-V Nitride Semiconductors and Material Systems—Physics and Technology*, edited by A. Erol Springer Series in Materials Science 105 (Springer-Verlag, 2008) Ch. 9, p. 222.
[32]M. Vandevyver and P. Plumelle, Phys. Rev. B **17**, 675 (1978).
[33]D. N. Talwar, M. Vandevyver, K. K. Bajaj, and W. M. Theis, Phys. Rev. B **33**, 8525 (1986).
[34]A. Grimm, A. A. Maradudin, I. P. Ipatova, and A. V. Subashiev, J. Phys. Chem. Solids **33**, 775 (1972).
[35]J. L. T. Waugh and G. Dolling, Phys. Rev. **132**, 2410 (1963).
[36]P. Plumelle and M. Vandevyver, Phys. Status Solidi B **78**, 271 (1976).
[37]D. N. Talwar, M. Vandevyver, K. Kunc, and M. Zigone, Phys. Rev. B **24**, 741 (1981).
[38]J. M. Rowe, R. M. Nicklow, D. L. Price, and K. Zanio, Phys. Rev. B **10**, 671 (1974).
[39]N. Vagelatos, D. Wehe, and J. S. King, J. Chem. Phys. **60**, 3613 (1974).
[40]J. C. Irwin and J. LaCombe, J. Appl. Phys. **45**, 567 (1974).
[41]W. A. Harrison, *Electronic Structure and the Properties of Solids* (Freeman, San Francisco, 1980).
[42]D. N. Talwar, K. S. Suh, and C. S. Ting, Philos. Mag. B **56**, 593 (1987).
[43]D. N. Talwar, Z. C. Feng, and P. Becla, Phys. Rev. B **48**, 17064 (1993).
[44]D. N. Talwar, M. Vandevyver, and M. Zigone, J. Phys. C **13**, 3775 (1980).
[45]G. W. Ludwig and H. H. Woodbury, in *Solid State Physics*, 2nd ed., edited by F. Seitz, D. Turnbull, and H. Ehreneich (Academic, New York, 1962), vol. 13, p. 223.
[46]A. Mujica, A. Rubio, A. Munoz, and R. J. Needs, Rev. Mod. Phys. **75**, 863 (2003).
[47]E. Deligoz, K. Colakoglu, and Y. Ciftci, Physica B **373**, 124 (2006).
[48]N. Jabari Lee, R. K. Kalia, A. Nakano, and P. Vashishta, App. Phys. Lett. **89**, 093101 (2006).
[49]D. N. Talwar (unpublished).
[50]A. D. Corso, S. Baroni, R. Resta, and S. de Gironcoli, Phys. Rev. B **47**, 3588 (1993).
[51]S. P. Gaur, J. F. Vetelino, and S. S. Mitra, J. Phys. Chem. Solids **32**, 2737 (1971).
[52]L. Bellomonte, J. Phys. Chem. Solids **38**, 59 (1977).
[53]J. A. Van Vechten and J. C. Phillips, Phys. Rev. B **2**, 2160 (1970).
[54]G. A. Baraff, E. O. Kane, and M. Schlüter, Phys. Rev. B **25**, 548 (1982).
[55]A. Mitsuishi, A. Manabe, H. Yoshinaga, S. Ibuki, and H. Komiya, Prog. Theor. Phys. Suppl. **45**, 21 (1970).
[56]B. K. Meyer, P. Omling, E. Weigel, and G. Müller-Vogt, Phys. Rev. B **46**, 15135 (1992).
[57]P. Emanuelsson, P. Omling, B. K. Meyer, M. Wienecke, and M. Schenk, Phys. Rev. B **47**, 15578 (1993).
[58]A. Carvalho, A. K. Tagantsev, S. Öberg, P. R. Briddon, and N. Setter, Phys. Rev. B **81**, 075215 (2010).
[59]S. Ibuki, H. Komiya, A. Mitsuishi, A. Manabe, and H. Yoshinaga, *Proc. Int. Conf. II-VI Semiconducting Compounds,* edited by D. G. Thomas (Benjamin, New York, 1967), p. 1140.
[60]R. Zielińska, A. Król, and W. Nazarewicz, J. Phys. C: Solid State Phys. **17**, 5209 (1984).